Smart Materials in Manufacturing 3 (2025) 100069

Contents lists available at ScienceDirect

Smart Materials in Manufacturing

journal homepage: www.keaipublishing.com/en/journals/smart-materials-in-manufacturing

Research Paper

A comprehensive study on the biodegradability, biocompatibility, and antibacterial properties of additively manufactured PLA-ZnO nanocomposites

Wei Juene Chong [a,b], Paul Wright [c], Dejana Pejak Simunec [b], Srinivasan Jayashree [b], Winston Liew [b], Chad Heazlewood [b], Adrian Trinchi [b], Ilias (Louis) Kyratzis [b], Yuncang Li [a], Shirley Shen [d], Antonella Sola [b,e,*], Cuie Wen [a,**]

[a] Centre for Additive Manufacturing, School of Engineering, RMIT University, Melbourne, Victoria, 3001, Australia
[b] CSIRO Manufacturing Research Unit, Clayton, Victoria, 3168, Australia
[c] School of Health and Biomedical Sciences, RMIT University, Bundoora, Victoria, 3083, Australia
[d] DSTG, Melbourne, Victoria, Australia
[e] Department of Sciences and Methods for Engineering, University of Modena and Reggio Emilia, 42122 Reggio Emilia, Italy

ARTICLE INFO

Keywords:
PLA
ZnO
Additive manufacturing
Antibacterial properties
Cytotoxicity

ABSTRACT

The addition of zinc oxide (ZnO) nanofillers to 3D printable poly(lactic acid) (PLA) filaments for material extrusion (MEX) additive manufacturing (fused filament fabrication, FFF, a.k.a. fused deposition modelling, FDM) has the potential to enable the fabrication of biomedical devices with embedded antibacterial functionality. This work investigates the biological properties, mainly the biodegradability, antibacterial activity, and cytotoxicity of 3D printed PLA-ZnO nanocomposites containing between 1 wt% to 5 wt% of either untreated or silane-treated filler. This study demonstrated that the concentration and surface properties of the filler control the matrix degradation rate, which directly influences the release rate of ZnO and Zn^{2+}, which in turn governs the antibacterial properties of the nanocomposites. All nanocomposites showed excellent antibacterial properties (> 99% reduction in bacteria) against both gram-positive (*Staphylococcus aureus*) and gram-negative (*Escherichia coli*) strains. Potential cytotoxic effects against human immune THP-1 cells were only evident at the highest filler loading (5 wt%), whereas nanocomposites with < 5 wt% filler loading were non-cytotoxic after 7 days of exposure. The 3D printed PLA-ZnO nanocomposites produced in this study show potential for use in clinical settings, with nanocomposites having filler loadings of < 2 wt% being the most appropriate candidates due to their excellent antibacterial properties while showing comparable biocompatibility to pristine PLA.

1. Introduction

Fused filament fabrication (FFF, a.k.a. fused deposition modelling, FDM), is one of the most popular material extrusion (MEX) techniques [1] in additive manufacturing (a.k.a. 3D printing) due to its economic accessibility, simplicity, and multi-material printing capabilities [2]. The integration of FFF with bio-based polymers that have intrinsic antibacterial properties allows for cost-effective customisation of biomedical devices, reducing contamination risks. Several commercially available antibacterial filaments, such as PLActive, Cicla, Bioguard, and Smartfil, are poly(lactic acid) (PLA)-based and functionalised with antibacterial nanomaterials like copper (Cu) and silver (Ag) [3–6]. However, the use of Cu and Ag nanoparticles presents significant limitations, including the high cost of Ag [7,8] and the potential cytotoxic effects of Cu [9,10]. Therefore, there is a continued need for more biocompatible and affordable antibacterial filaments.

One promising alternative is offered by PLA-zinc oxide (PLA-ZnO) nanocomposites, which exhibited excellent antibacterial properties against a broad spectrum of bacteria, primarily for applications in food packaging and wound healing [11–13]. Recent efforts have focused on

Peer review under the responsibility of Editorial Board of Smart Materials in Manufacturing.
* Corresponding author. Department of Sciences and Methods for Engineering, University of Modena and Reggio Emilia, 42122 Reggio Emilia, Italy.
** Corresponding author. Centre for Additive Manufacturing, School of Engineering, RMIT University, Melbourne, Victoria, 3001, Australia.
E-mail addresses: antonella.sola@unimore.it (A. Sola), cuie.wen@rmit.edu.au (C. Wen).

https://doi.org/10.1016/j.smmf.2024.100069
Received 29 August 2024; Received in revised form 10 October 2024; Accepted 16 October 2024
Available online 2 November 2024

expanding PLA-ZnO applications in healthcare by engineering the material for additive manufacturing, enabling the creation of complex geometries tailored to patients' needs [14]. Unlike conventional fabrication methods that often limit structural complexity, 3D printed PLA-ZnO nanocomposites enable the manufacture of intricate designs, enhancing their functionality in biomedical applications. Various studies have investigated the development of PLA-ZnO filaments for FFF [15–19], with some confirming the material's printability [15,17,19]. However, the main challenge is the elevated processing temperatures during filament fabrication and printing, which can lead to PLA degradation catalysed by ZnO, negatively impacting the nanocomposites' properties [20–22].

Despite this hurdle, the processability of PLA-ZnO can be improved by surface treating the filler with silane and using the 'masterbatch' fabrication technique, both of which minimise ZnO's degradative impact [22–25]. For the first time, these strategies were applied in a printability study by the authors' group [21], which examined the effects of ZnO concentration (1 wt% to 5 wt%), surface treatment (silanised vs. untreated ZnO), and masterbatch mixing strategy (solvent vs. melt mixing) on thermal, rheological, and mechanical properties relevant to printability. Results indicated that better printability was achieved with lower filler loadings and surface-treated ZnO, while melt-mixed masterbatches demonstrated superior filler dispersion due to high shear mixing.

Building on our previous study [21], this work aims to investigate the biological properties: biodegradability, biocompatibility, and antibacterial properties, of 3D printed PLA-ZnO nanocomposites. The specific objective is to determine the optimal concentration and surface treatment of the filler needed to balance printability, antibacterial efficacy, and biocompatibility. This study represents the first comprehensive assessment of the biological properties of FFF-printed PLA-ZnO nanocomposites, focusing on the effects of filler loading (1 wt% to 5 wt%), filler treatment (silanised vs. untreated), and the interplay between matrix degradation and Zn^{2+} release rates on antibacterial properties and cytotoxicity. This research could facilitate the adoption of PLA-ZnO nanocomposites for 3D printing a variety of antibacterial and biocompatible biomedical devices for medical implants, tissue engineering, and surgical procedures.

2. Materials and methods

2.1. Fabrication of test specimens

Ingeo 3D850 PLA pellets, a grade formulated for extruding filaments for additive manufacturing, were acquired from NatureWorks LLC (Minnetonka, MN, USA). The technical datasheet of the as-received pellets specified a melt flow rate of 0.7–0.9 g/min at 210°C and a density of 1.24 g/cm^3 [26]. Nanosun Zinc Oxide P99/30 was kindly supplied by Micronisers (Dandenong, VIC, Australia). The technical datasheet of the as-received powder specified a mean particle size between 30 and 50 nm, and a bulk density of 0.3 g/cm^3, with a purity greater than 99.5% [27]. 3-Aminopropyltriethoxysilane (APTES) (CAS no. 919-30-2) used for the surface treatment of ZnO was purchased from Sigma Aldrich (St. Louis, MO, USA).

Disc-shaped test specimens of PLA and PLA-ZnO nanocomposites (10 mm diameter and 5 mm height) were 3D printed from filaments fabricated according to the procedure developed by the authors' group [21]. In brief, the neat PLA filaments were produced via melt-extrusion of pristine PLA pellets, whereas the nanocomposite filaments were produced via melt-compounding of pristine PLA pellets with masterbatches prepared by melt-mixing of PLA with 10 wt% of either untreated or APTES-treated ZnO (hereinafter referred to 'treated ZnO'). The printability assessment previously completed by the authors' group showed that filaments produced from melt-mixed masterbatches achieved better properties and more homogeneous filler dispersion than those produced from solvent-mixed masterbatches [21]. Hence, only the filaments obtained from melt-mixed masterbatches were used for the biological characterisations in this study.

For the sake of comparison, the commercially available antibacterial Bioguard filaments (PLA-Ag filaments) were purchased from 3DXTECH (Chicago, IL, USA) to 3D print test specimens for biocompatibility and antibacterial testing. All the material formulations used in this work are detailed in Table 1.

A commercial FFF printer (Raised 3D Pro 2) was used to print a total of at least 36 discs-shaped specimens (10 mm diameter and 5 mm height) per material type in accordance with the print parameters listed in Table 2. The specimens were printed in batches of 12 per material type at a time.

2.2. Sterilisation of test specimens

All printed disc specimens were sterilised by soaking in 80% ethanol for 5 min and air-dried in a class II biological safety cabinet prior to biological characterisation studies.

2.3. Evaluation of biodegradability

The biodegradation rates of the discs were determined by measuring the amount of lactic acid (LA) released in two different types of immersion media: Milli-Q water (H_2O) acidified to a pH of 5.5 by pre-incubation at 37°C in a cell culture incubator with humidified air with 5% CO_2; and Gibco Minimum Essential Medium (MEM, Life Technologies, Thermo Fisher Scientific) at pH 7.4. An aliquot (2 mL) of either medium was pipetted into the individual wells of a 24-well plate, with each well containing a sterilised disc. The wells containing the neat PLA discs served as the control group of the study. The plates were incubated at 37°C in humidified air with 5% CO_2 for the following time points: 1 day (24 h), 1 week (168 h), 2 weeks (336 h), 4 weeks (672 h), 7 weeks (1176 h), 10 weeks (1680 h), and 12 weeks (2016 h). At each sampling time point, the media was collected from each well and replaced with fresh liquid. Subsequently, half of the collected sample from each well (1 mL) was used for measuring the LA concentration, whereas the other half was processed to measure the Zn^{2+} release as described in the following section (Section 2.4).

Ultra-performance liquid chromatography (UPLC) (Acquity UPLC H-Class PLUS, Waters Corporation, Milford, MA, USA) equipped with Acquity UPLC HSS T3 column (50 × 2.1 mm, 1.8 μm particle size) was used to detect the LA released in the immersion media. The analytical detector was a Waters Photodiode Array (PDA) detector which was set to a wavelength ranging from 190 to 400 nm, with chromatograms extracted at 210 nm. Chromatographic separation was carried using a gradient elution with 100% Milli-Q water with 0.1% formic acid and 100% acetonitrile with 0.1% formic acid as mobile phase A and B, respectively. The gradient program was as follows: hold at 100 % A for 1 min; 100% A to 100% B over 3.5 min, hold at 100% B for 1 min; change to 100% A over 5 min; hold for 1 min. The column temperature was set at 30°C with a flow rate of 0.4 mL/min. The injection volume for each

Table 1
Material formulations investigated in this study. The actual filler loading is based on experimental results published separately for the PLA-ZnO filaments [21], and is taken from the manufacturer's datasheet for Bioguard [5].

Disc sample ID	Filler type	Filler loading (wt%)	
		Nominal	Actual
PLA	n/a	n/a	n/a
1M	ZnO	1	2.0 ± 0.1
3M	ZnO	3	4.0 ± 0.1
5M	ZnO	5	5.1 ± 0.1
1MT	Treated ZnO	1	1.7 ± 0.1
3MT	Treated ZnO	3	3.9 ± 0.1
5MT	Treated ZnO	5	4.6 ± 0.2
Bioguard (commercial)	Ag	n/a	< 2%

Table 2
Processing parameters used for printing the test specimens for all the material formulations listed in Table 1.

Print parameter	Value
Infill density	100%
Infill flowrate	100%
Infill pattern	Concentric
First layer thickness	0.3 mm
Layer thickness	0.2 mm
First layer print speed	30 mm/s
Layer print speed	80 mm/s
Nozzle temperature	230°C
Bed temperature	60°C
Build orientation	x-y plans (flat)
Nozzle diameter	0.4 mm

sample was 1 μL.

The concentration of LA was determined using calibration standards ranging from 0.01 to 100 mg/mL run in triplicates in both H_2O and MEM. The LA peak area at 210 nm were measured in Waters Empower software using an automatic processing method, and the average area of the three injections was used. Lower calibration range curves were constructed in the range 0.01–10 mg/mL, and higher range calibration curves were constructed in the range 5–100 mg/mL for both H_2O and MEM, for both Peak 1 and Combined Peaks. The trendline equations for each calibration curve were calculated using Microsoft Office Excel software, with linear equations used for the lower range curves and quadratic equations used for the higher range curves, and an $R^2 > 0.999$ was found for all curves.

2.4. Evaluation of Zn^{2+} release

The Zn^{2+} release assay was performed in parallel to the biodegradation assay using the same set up described in Section 2.3 but with additional time points at 4 h, 3 days (72 h), and 3 weeks (504 h). The 1 mL aliquot of soaking medium collected from each well as described in Section 2.3 was then acidified with 2% v/v nitric acid prior to the Zn^{2+} measurement.

Inductively coupled plasma mass spectrometry (ICP-MS) (8900 Triple Quadrupole 8900 ICP-MS, Agilent, Santa Clara, CA, USA) was used to determine the concentration of Zn^{2+} present in the immersion media after the specified incubation time points. The accuracy of the calibration and the method of measurement were verified using certified multi-element solutions (QCS-27-100, High Purity Standards, North Charleston, SC, USA).

The obtained cumulative Zn^{2+} release data was then analysed with zero-order, first-order, Higuchi, and Korsmeyer-Peppas models using Equations (1)–(4) [28].

Zero order:

$$Q_t - Q_o = Kt \tag{1}$$

Q_t is the concentration of Zn^{2+} released at time t; Q_o is the initial concentration of Zn^{2+} released; K is zero-order release rate constant.

First-order:

$$ln\, C_o - ln\, C_i = Kt \tag{2}$$

C_o is the initial concentration of Zn^{2+} in the samples; C_i is the concentration of Zn^{2+} released at time t; K is the first-order release rate constant.

Higuchi:

$$Q_t = K_H t^{0.5} \tag{3}$$

Q_t is the concentration of Zn^{2+} released at time t; K_H is the Higuchi release constant.

Korsmeyer-Peppas:

$$\frac{M_t}{M_\infty} = Kt^n \tag{4}$$

$\frac{M_t}{M_\infty}$ is the concentration of Zn^{2+} released at time t; K is the release constant; n is the diffusional exponent.

2.5. Evaluation of in vitro cytotoxicity

The human acute monocytic leukemia (THP-1) cell line was kindly provided by the Department of Medicine, University of Melbourne, Melbourne, Australia, and cultured in RPMI-1640 medium containing 300 mg/L L-glutamine, 100 IU/mL penicillin, 100 μg/mL streptomycin and 10% (v/v) fetal bovine serum, all purchased from Gibco (Life Technologies, ThermoFisher Scientific, Waltham, MA, USA).

The cell viability studies were performed under sterile conditions as per O'Keefe et al. [29], with the following modifications. In brief, 10^5 cells in 2 mL of culture media were incubated with a sterilised disc in each well of a 24-well plate at 37°C in humidified air with 5% CO_2 for 1, 3, and 7 days. Exposures were performed using four replicate wells for each incubation condition. Unexposed cells were employed as the negative control, while cells exposed to 5% dimethyl sulfoxide (DMSO) were used as the positive cytotoxicity control of this study. At the sampling time points, the discs were removed from the wells and the cells carefully resuspended by mixing using a 1 mL pipette tip. Immediately after mixing, two 200 μL aliquots of cell suspension were transferred to separate wells in a 96-well plate. The exposed cells in each well were then treated with 40 μL of 3-(4,5-dimethylthiazol-2-yl)-5-(3-carboxymethoxyphenyl)-2-(4-sulfophenyl)-2H-tetrazolium reagent (MTS, Promega MTS CellTiter 96 aqueous kit, Madison, MI, USA) and the extent of formazan formation after 4 h of incubation at standard growth conditions was compared to that of an unexposed control group, by measuring the absorbance at a wavelength of 490 nm using a plate reader (CLARIOstar, BMG Labtech, Ortenberg, Germany). The absorbance of each sample well was averaged across duplicate wells, prior to being divided by the average absorbance of the wells containing unexposed cells in media, to provide cell viability values as a percentage of control cell viability.

2.6. Evaluation of antibacterial activity

The gram-positive bacteria *Staphylococcus aureus* (*S. aureus*) NCTC 10788 on BioBall Multishot 10E8 were purchased from bioMériux (Marcy-l'Étoile, France), with each BioBall containing 10^8 colony-forming units (CFU) according to the supplier's datasheet [30]. To prepare the *S. aureus* test inoculum, the BioBall was dissolved in 1.1 mL of 2x Yeast Extract Tryptone (2x YT, consists of 1.6% Tryptone, 1% yeast extract and 0.5% sodium chloride) broth in a tube, mixed for 5 s and then diluted with sterile H_2O to a 1:167 ratio, achieving a concentration of approximately 6 x 10^5 CFU/mL.

The gram-negative bacteria *Escherichia coli* (*E. coli*) ATCC 25922 on Culti-Loops were purchased from Thermo Fisher Scientific (Waltham, MA, USA). For the *E. coli* test inoculum, a seed culture was prepared by streaking a bacterial loop on a warm nutrient agar plate and incubating at 37°C for 24 h. An isolated colony was inoculated into 100 mL of 2x YT broth in a baffled flask, loosely covered, and incubated at 37°C with shaking at 200 rpm for 16 h. The obtained seed culture was then diluted with sterile H_2O to achieve a concentration of approximately 6 x 10^5 CFU/mL.

Subsequently, a sterilised disc was placed in a 50 mL test tube and submerged in 3 mL of the prepared inoculum. All the test tubes were capped with perforated lids and incubated at 37°C with shaking at 200 rpm for 24 h. Unexposed cultures served as the negative control, whereas cultures exposed to Bioguard discs acted as positive antibacterial controls. After incubation, an aliquot was drawn from each test tube and serially diluted 10-fold in phosphate-buffered saline (PBS)

down to a 10^{-6} dilution of the neat aliquot. 100 μL of each dilution were plated on agar plates and incubated at 37°C overnight prior to CFU quantification. The antibacterial activity index (A) of the materials was then determined based on Equation (5) adopted from previous studies [25,31], where F represents the growth values obtained from pristine PLA samples, and G represents the growth values from the nanocomposites. The growth values of the materials were calculated based on their respective CFU measurements as follows: log CFU_{24h} – log CFU_{0h}.

$$A = F - G \tag{5}$$

2.7. Characterisation of surface morphology

Field emission-scanning electron microscopy (FE-SEM) (Zeiss Merlin, Zeiss, Oberkochen, Germany) was used to characterise the changes in the surface morphology of the discs throughout the biodegradability assessment (Section 2.1). All samples were mounted on aluminium stubs and coated with iridium to a thickness of 5 nm, and characterised with an accelerating voltage of 5 kV. X-ray energy dispersive spectroscopy (EDS) was then employed to identify the chemical elements of the samples using the X-Max Extreme 100 mm^2 windowless Silicon Drift Detector (SDD, Oxford Instruments, Abingdon, UK). An accelerating voltage of 5 kV was applied for the EDS analysis.

2.8. X-ray diffraction (XRD)

An X-ray diffractometer (SmartLab, Rigaku, Tokyo, Japan) equipped with a rotating anode CuKα source (45 kV, 200 mA) and Hypix 3000 detector was employed to assess the crystallinity of the discs before and after immersion in media, to evaluate the impact of biodegradation on the matrix crystallinity of the discs. For all the discs, data was collected over a 5°–90° 2θ range with a step size of 0.04° and a scan rate of 2° per min. The collected data was analysed using the Bruker XRD search match program EVA 7, and crystalline phases were identified through the ICDD-JCPDS powder diffraction database.

2.9. Statistical analysis

All experiments were performed using at least three replicates for all exposure conditions, and the data is represented as the mean of at least three replicates ± standard error of the mean (SEM). Results were subjected to one-way ANOVA (or two-way ANOVA where appropriate), and Bonferroni post hoc test (SPSS Statistics, IBM, Armonk, NY, USA). A p-value <0.05 was used to identify statistically significant differences between groups.

3. Results and discussion

3.1. Biodegradability

PLA in aqueous environments degrades primarily through hydrolysis, which is a process where water molecules cleave the ester bonds of PLA, leading to a progressive loss in molecular weight and to the release of degradation products such as short oligomers and monomers [32]. In this study, the different biodegradation rates of the printed samples were quantified by measuring the concentration of LA (the monomer of PLA [33]), released in either H_2O (Fig. 1) or MEM (Fig. S1) over a maximum time of 12 weeks (2016 h).

Surface degradation and bulk degradation are the two main forms of

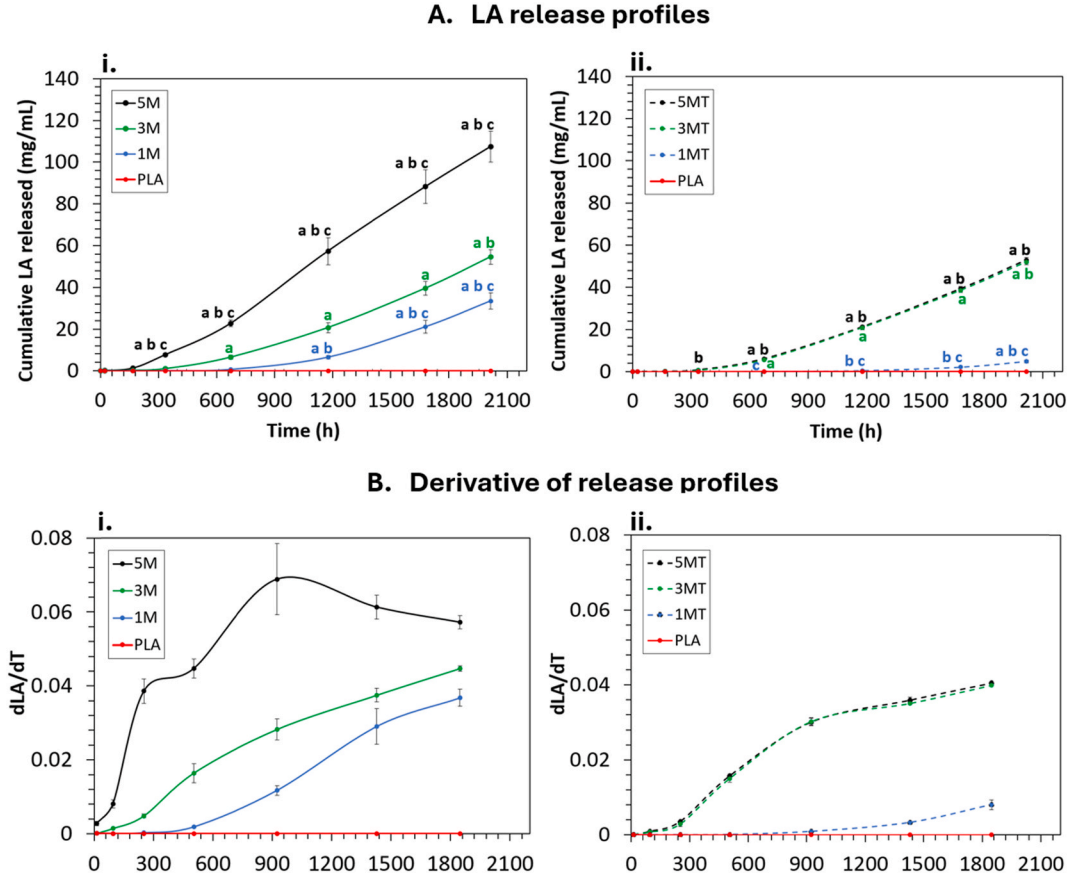

Fig. 1. Cumulative (A) and associated derivative (B) LA release profiles of the nanocomposites in H_2O for untreated fillers (i) and treated fillers (ii) (data expressed as the mean ± SEM of three replicates). Notes: [a] significantly different to PLA; [b] significantly different between treated and untreated ZnO with the same filler loading; [c] significantly different to the rest of the nanocomposites within the same filler surface treatment group.

polymer degradation. The former process is limited to the surface of the sample and occurs when the hydrolysis rate is higher than the water diffusion rate, leading to thinning of the sample while maintaining its bulk integrity [34]. The latter occurs throughout the sample when the rate of water penetration is faster than the rate of degradation [34]. In bulk degradation, the mass and the dimension of the sample are preserved for a period of time until a critical point is reached where the molecular weight significantly decreases, leading to the rapid release of oligomers and monomers [35].

As shown in Fig. 1, pristine PLA exhibited limited degradation even after 12 weeks. However, the addition of ZnO led to the bulk degradation of PLA, as indicated by the LA release profiles of the nanocomposites. Initially, there was a slow release of LA, which was followed by a rapid increase, particularly noticeable in 5M, before eventually declining after reaching its peak (as shown in Fig. 1B(i)).

This LA release behaviour of the nanocomposites suggests that degradation affects the entire sample rather than just the surface. Upon immersion, water diffused into the discs, facilitated by structural voids inherent to the FFF printing process, as seen in the FE-SEM micrographs presented in Fig. 2 and Fig. S2, day 0 (before immersion). Initially, low concentrations of oligomers and monomers were released due to the sufficiently entangled polymer chains, which restricted the diffusion of degradation products [36,37]. However, as chain cleavage progressed, the reduced chain length increased mobility and formed hydrophilic end groups in PLA (e.g. carboxyl groups), promoting water uptake and resulting in substantial swelling of the matrix.

As degradation continued, more degradation products formed both on the surface and in the core of the samples. The degradation products in the core diffused less readily, creating a localised acidic environment that further catalysed degradation through 'autocatalysis' [38]. This led the nanocomposites to degrade more rapidly in the core, consequently forming a sort of less degraded 'outer shell' surrounding the generated monomers and oligomers [38]. Once a critical molecular weight was reached, these degradation products rapidly diffused out of the bulk [39], aligning with the second stage of accelerated LA release observed after at least 1 week, as shown in Fig. 1.

As noted earlier, the LA release rate of 5M decreased after reaching its maximum. Similarly, the degradation rates for other nanocomposites, except 1MT (Fig. 1(ii)), also slowed towards the end of the experiment. This decline was attributed to the depletion of degradation products in

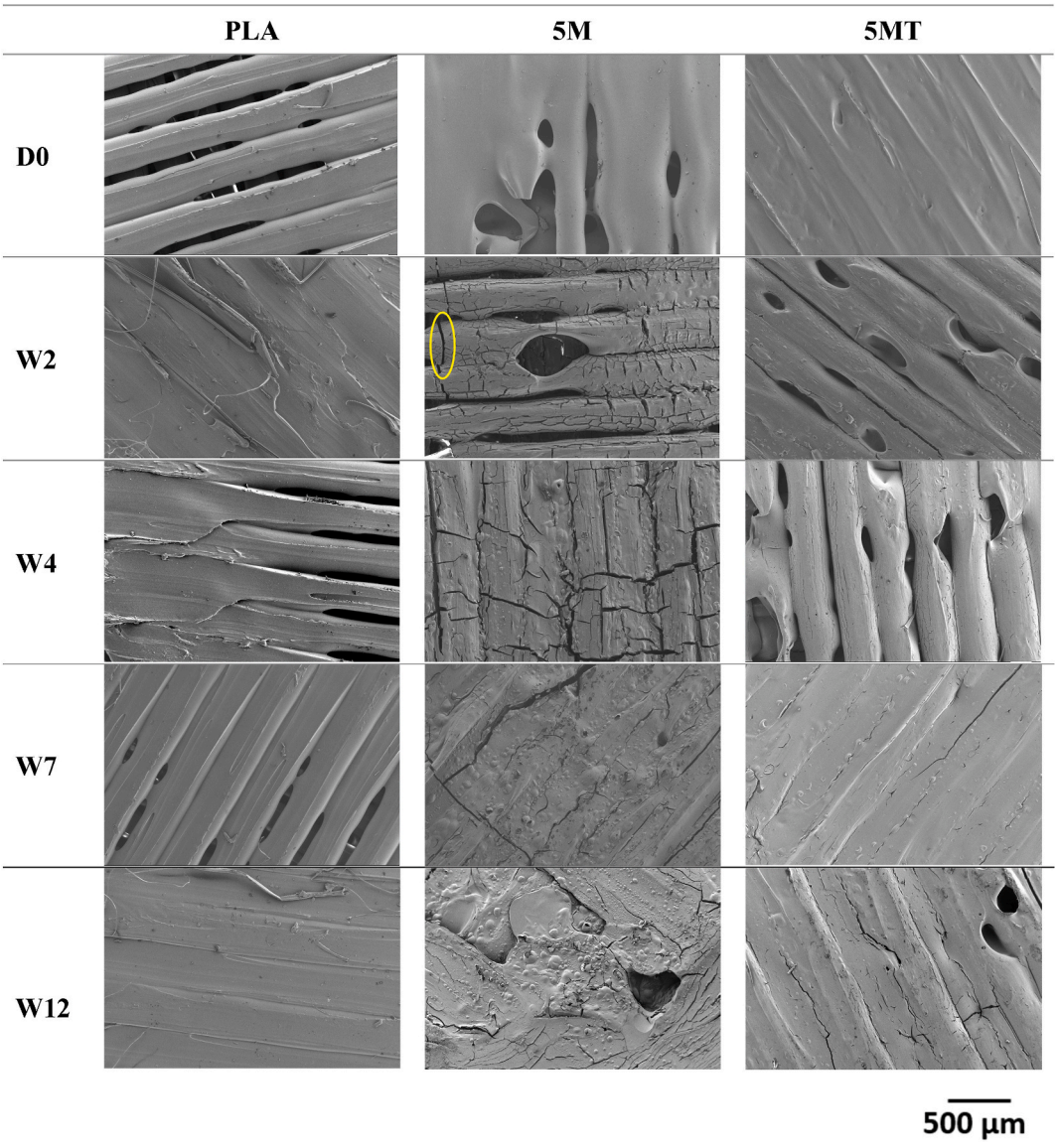

Fig. 2. Surface morphology of neat PLA and PLA-ZnO nanocomposites before and after 12 weeks of degradation in H2O (x40 magnification). Yellow circle: example of cracks that cut perpendicularly to the rasters. Scale bar: 500 µm for all the micrographs.

the core, which reduced the autocatalytic degradation of the polymer [38]. Additionally, increased crystallinity of the polymer matrix, due to the enhanced mobility of the short and loosely entangled molecular chains, may have reduced the degradation rate [40]. Higher crystallinity reduces the amorphous regions that are particularly sensitive to degradation [41], and is often characterised by increased opacity over time [42], for example as shown by 1M (Fig. 3). This crystallisation was further confirmed by the XRD results as exemplified in Fig. S4 for 1M.

Changes in surface morphology, along with LA release profiles, validate the bulk degradation mechanism of the samples. Fig. 2 and S2 exemplifies these morphological changes with increasing immersion time, while Fig. S3 provide higher magnification views. A key feature of bulk degradation is the formation of cracks and crevices due to swelling and dissolution of the polymer [43–45]. After 2 weeks, all the nanocomposites exhibited obvious microcracks that widened and deepened over time (Fig. 2 and S2).

The extent of matrix degradation is clearly dependent on the filler loading, with 5M exhibiting the fastest degradation (5M > 3M > 1M). This is evidenced by the increasing LA release rates and the magnitude of crack formation. For instance, 5M, with the highest filler loading, not only experienced the higher LA release rates but also displayed the fastest crack formation, with some rasters (i.e. the printed strands of material that are the fundamental structural unit of FFF parts [46]) completely severed after 2 weeks of immersion (yellow circle in Fig. 2). This rapid crack growth facilitates water penetration and the diffusion of degradation products from the matrix, correlating with the significant increase in LA release from 5M after the first week. This allowed 5M to reach the critical molecular weight necessary for the substantial release of degradation products from the core, making it the first to experience reduced autocatalysis.

This phenomenon is primarily related to the catalytic role of ZnO in the chain cleavage of PLA, due to the abundant hydroxyl groups on the surface of ZnO [47,48]. Our previous study [21] confirmed that increasing filler loading increases the thermal degradation of PLA during extruding and printing, resulting in lower molecular weights and reduced chain entanglement. As a consequence, the loosely entangled chains in the nanocomposites can be easily separated and plasticised by water molecules, inducing swelling of the matrix which further accelerates water absorption and hydrolysis [49]. Additionally, water diffusion is facilitated by the interfacial voids arising from the poor compatibility between PLA and untreated ZnO [50]. ZnO also enhances the hydrophilicity of PLA [51,52], further increasing the matrix's water absorption capacity and accelerating hydrolysis.

Treated ZnO significantly reduces the degradation of the nanocomposites, as evidenced by the lower LA release rates shown in Fig. 1. For instance, 1MT (treated ZnO) and 5MT (treated ZnO) released less LA than their untreated counterparts starting from the 7th week (1200 h) and the 2nd week (336 h), respectively. This is attributed to silane's ability to mitigate the catalytic effect of ZnO on the processing-induced PLA degradation by partially replacing the strongly hydrophilic hydroxyl groups of the fillers with O-Si bonds [53], increasing the molecular weight and chain entanglement of the printed nanocomposites, as reported in our previous study [21]. Moreover, silane contains functional groups that form stable bonds with both PLA and ZnO, improving interfacial adhesion and reducing water penetration at the matrix-filler region [54]. As a result, silane limits polymer mobility, reduces solvent penetration and decreases matrix swelling [55], collectively improving resistance to hydrolytic degradation.

Fig. 3. Test specimen of 1M (left) before immersion and (right) after 4 weeks of degradation in H_2O. Scale bar: 5 mm.

Treated fillers thus provide better protection against matrix degradation, delaying crack formation, for example, as seen in the smaller cracks on the surface of 5MT as compared to 5M after 2 weeks of immersion (Fig. 2). Furthermore, silane minimises the impact of filler loading on the biodegradation rates of the samples, as shown by the similar biodegradation rates between 3MT and 5MT. This similarity is partially attributed to their comparable (actual) filler loadings (3.9 wt% for 3MT vs. 4.6 wt% for 5MT [21]) and the more stable molecular weights achieved through silane's ability to mitigate ZnO-induced processing degradation of PLA (123 kDa for 3MT vs. 124 kDa for 5MT [21]). Both of these factors likely explain the similar biodegradation rates observed.

While silane treatment enhances the physical (mechanical, thermal, and rheological) properties of the nanocomposites [21], its effectiveness in reducing degradation rates in aqueous environments varies by filler loading. For instance, 3MT (treated ZnO) and 3M (untreated ZnO), which had similar filler loadings, exhibited comparable LA release rates regardless of surface treatment (Fig. 1). Notably, our previous work demonstrated that 3MT exhibited superior matrix properties and thermal stability due to the reduced processing-induced PLA degradation [21], suggesting that factors beyond filler hydrophilicity and chain entanglement density, such as crystallinity, may influence water uptake and hydrolysis.

Crystallinity affects water diffusion in thermoplastics like PLA; increased crystallinity generally reduces amorphous regions that facilitate water diffusion [41]. However, Tsuji and Del Carpio [56] noted that highly crystalline polymers may experience accelerated hydrolysis. In such cases, the terminal carboxyl and hydroxyl groups excluded from the crystalline regions of the polymer accumulate in the amorphous regions. Consequently, the residual amorphous regions between the crystalline phases become densely packed with highly hydrophilic terminal groups, potentially accelerating water diffusion into the polymer at higher rates than those seen in polymers with larger amorphous regions [56].

Our prior research showed that crystallisation was impaired in nanocomposites with >2 wt% untreated filler due to the high concentration of chain end groups acting as defects [21]. Hence, the nanocomposites with treated ZnO attained higher crystallinity at filler loadings >2 wt%: 3MT (29%) compared to 3M (23%), and 5MT (31%) compared to 5M (25%). In contrast, nanocomposites with < 2 wt% filler loadings, i.e., both 1MT and 1M, displayed similar crystallinity (~27%) regardless of surface treatment [21].

The effect of silane in reducing ZnO-driven water affinity is evident in the significant reduction of LA released from 1MT compared to 1M, where the impact of crystallinity on water uptake can be disregarded. However, for filler loadings >2 wt%, silane treatment reduced filler hydrophilicity, but this effect was counterbalanced by increased crystallinity according to the model proposed by Tsuji and Del Carpio [56], explaining the statistically similar degradation rates between 3MT and 3M. Nonetheless, when the filler loading increased further to 5 wt%, the beneficial effect of silane became apparent again (Fig. 1), as improved filler-matrix compatibility and increased chain entanglement enabled the so-called "tortuosity effect", where fillers restrict water diffusion [57], with this effect becoming more pronounced at greater filler loadings [49,58]. Thus, with approximately 5 wt% of treated ZnO, the tortuosity effect outweighed the impact of increased crystallinity, leading to an overall decrease in water uptake, which led to the lower degradation rates observed for 5MT compared to 5M.

Additionally, the type of immersion media, whether the unbuffered acidic pH of H_2O (Fig. 1) or the buffered physiological pH of MEM (Fig. S1), did not substantially alter the degradation rates of the samples despite the differences in pH. This lack of noticeable effect aligns well with previous studies [59–62], which often associated the insensitivity to pH to the complex mechanisms governing polymer degradation. In this context, each medium catalysed the hydrolysis of PLA in distinct ways immediately upon the immersion. For instance, samples immersed in H_2O, which has a relatively low ionic strength, experienced greater osmotic pressure, potentially enhancing water uptake and thereby increasing degradation rates. On the other hand, the initial degradation rates of the samples in MEM may be elevated by the neutralisation effect of the buffer solution on the acidic degradation products. As explained by Hurrel and Cameron [38], this neutralisation shifts the equilibrium toward creating more products, consequently accelerating the degradation rate.

Nonetheless, after some time, degradation in both media was predominantly controlled by autocatalysis, which is primarily influenced by the internal acidity of the samples rather than the external environment. Moreover, the effect of environmental pH on PLA degradation usually becomes significant only under more extreme pH conditions, such as strongly alkaline environments around pH 10 and above [63, 64]. Thus, the effect of the pH of the media has a negligible effect on the samples' internal acidity, leading to the similar degradation rates across both media.

3.2. Zn^{2+} release rates

Fig. 4 shows the cumulative concentration and the corresponding cumulative percentage of Zn^{2+} released in H_2O. For the sake of simplicity, the Zn^{2+} measurements determined in MEM have been included in Fig. S5. For pristine PLA, less than 0.1 mg/mL of Zn^{2+} were detected in the immersion liquid throughout the experimental immersion times.

All the nanocomposites did not exhibit distinct initial burst release, indicating that most ZnO nanoparticles were embedded within the matrix. The cumulative Zn^{2+} release profiles followed a trend similar to the LA release, showing an initial slow release phase, during which less than 10% of the total Zn^{2+} mass loading was released (Fig. 4B), followed by a rapid release phase. Zn^{2+} release continued for at least 12 weeks, with higher Zn^{2+} concentrations released at increasing filler loadings, but reduced in the presence of silane treatment except at 3 wt% filler loading. This trend release closely mirrors the LA release profiles, indicating that the same mechanisms governing the LA release, as previously described in Section 3.1, also apply to the Zn^{2+} release, with both being affected by filler concentration and surface treatment in a similar manner.

To understand the Zn^{2+} release mechanism, the data was fitted to common mathematical models including the zero-order, first-order, Higuchi, and Korsmeyer-Peppas models, with the last model being only valid for the first 60% of the total drug/filler released [28]. The coefficient of determination (R^2) and release rate constants obtained from the kinetic models are presented in Table 3.

The Korsmeyer-Peppas model's diffusion exponent (n-value) predicts the release mechanism of polymeric systems and is influenced by the geometry of the system. For this study involving cylindrical samples, $n > 0.89$ indicates Super Case II transport, where the release is primarily controlled by matrix degradation [65,66]. Most nanocomposites exhibited Super Case II transport, except for 1MT, which demonstrated anomalous transport ($0.45 < n < 0.89$), suggesting that the Zn^{2+} release

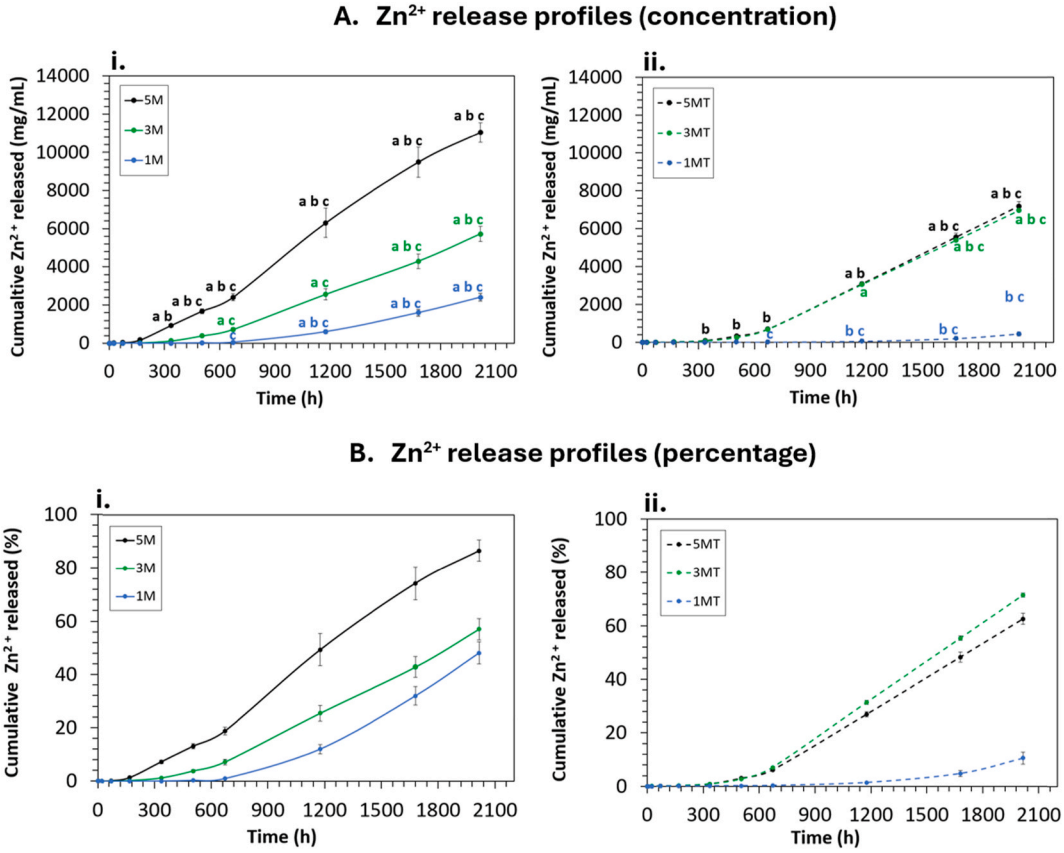

Fig. 4. Cumulative concentrations (A) and percentages (B) of Zn^{2+} released in H_2O for (i) untreated fillers and (ii) treated fillers (data expressed as the mean ± SEM of three replicates). Notes: [a] significantly different to PLA; [b] significantly different between treated and untreated ZnO within the same filler loading; [c] significantly different to the rest of the nanocomposites within the same filler treatment group.

Table 3
The Zn^{2+} release kinetic parameters in H_2O derived from the different mathematical models.

Sample	Zero-order	First-order	Higuchi		Korsmeyer-Peppas	
	R^2	R^2	R^2	K_H	R^2	n
1M	0.87	0.84	0.47	0.15	0.80	1.19
1MT	0.79	0.77	0.70	0.02	0.89	0.66
3M	0.95	0.92	0.65	0.40	0.92	1.34
3MT	0.94	0.90	0.58	0.45	0.85	1.17
5M	0.98	0.93	0.78	0.89	0.95	1.36
5MT	0.94	0.91	0.60	0.4	0.89	1.28

from 1MT is more dependent on diffusion and matrix swelling rather than degradation [67,68]. This anomaly is likely attributed to the low filler loading and filler treatment of 1MT, which in turn limit the extent of matrix degradation's role on its Zn^{2+} release mechanism.

Notably, Fig. 5 reveals a slight burst of Zn^{2+} release during the initial release phase of 1MT, during which diffusion was likely the governing mechanism. Consequently, 1MT released higher amounts of Zn^{2+} than its untreated counterpart (1M) up to the 1st week (168 h) (detail shown in Fig. 5). The low degree of filler agglomeration in 1MT may have facilitated easier nanofiller diffusion out of the matrix [69], resulting in higher amounts of Zn^{2+} detected at the early stages of the experiment prior to matrix degradation. Importantly, matrix degradation did not contribute to the initial burst release of 1MT, as it consistently released lower LA concentrations compared to 1M throughout the experiment (Fig. 1).

While empirical and semi-empirical mathematical models can provide insights into predominant release mechanisms, they often fail to accurately interpret the release kinetics of degradable polymer-based systems, as they do not encompass all the involved physical processes [70]. The optimisation of these models for simulating polymeric system release mechanisms is complex and has been extensively discussed in the literature [70–73]. According to Siepmann et al. [70], these models tend to conflate various mass transport mechanisms related to degradable matrices, such as diffusion, swelling, and degradation, potentially resulting in an overall zero-order release profile. Given the strong correlation of the nanocomposites with the zero-order model (as indicated by the R^2 values in Table 3), it is reasonable to conclude that the interplay of diffusion, swelling, and degradation influenced the release of Zn^{2+} from the nanocomposites in this study.

During the initial slow-release phase, diffusion predominated. Water penetrated the matrix upon contact, enhancing chain mobility which transformed the polymer to a swollen, rubbery state [74]. Concurrently, the embedded ZnO dissociated into Zn^{2+} and diffused out of the swollen

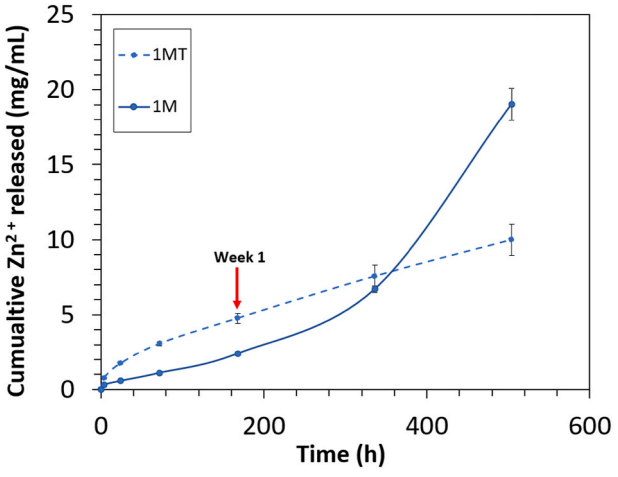

Fig. 5. Cumulative concentration of Zn^{2+} released from 1 MT to 1M up to 3 weeks (504 h).

polymeric network [75]. The slight decrease in Zn^{2+} release rate observed for 5M approximately between the 3rd (504 h) and the 4th week (672 h) (Fig. 4) is likely due to the lengthening of the Zn^{2+} diffusion path caused by the swollen matrix [76].

As water absorption continued, polymer degradation commenced, leading to chain cleavage into oligomers and monomers [32]. This process created cracks and pores, facilitating the release of oligomers and monomers, which in turn accelerated Zn^{2+} release [77]. The onset of rapid Zn^{2+} release (Fig. 4) coincides approximately with the onset of the accelerated LA release (Fig. 1), confirming that matrix degradation played a significant role in the rapid release of Zn^{2+}, consistent with the Super Case II mechanism observed in of most of the nanocomposites in this study.

Following the maximum release rate, the gradual decline in Zn^{2+} release from 5M (Fig. 4) mirrored its degradation profile (Fig. 1), due to the reduction in autocatalytic degradation as discussed in Section 3.1. The prevalence of matrix degradation in Zn^{2+} release explains why the filler loading and the filler treatment affected the Zn^{2+} release rates similarly to the LA release rates.

Interestingly, the type of immersion media significantly influenced Zn^{2+} release rates in the nanocomposites, more so than the degradation rates (LA release) discussed in Section 3.1. Statistical analysis showed no significant interaction between media type and LA release. However, for Zn^{2+} release, a significant interaction was observed, with concentrations in MEM taking one week longer than in H_2O to reach statistical significance (Fig. S5). This suggests lower Zn^{2+} release rates in MEM, independent of matrix degradation. The difference may stem from the higher solubility of ZnO in the more acidic H_2O (pH 5.5) compared to MEM (pH 7.4) [78]. The increased hydrogen ion (H^+) concentration in H_2O enhances ZnO dissolution (Equation (6)) [78,79]. Furthermore, H^+ can react with hydroxide ions (OH^-) (Equation (7)), generating additional water and promoting ZnO dissociation into Zn^{2+}. Thus, the acidic environment of H_2O results in higher Zn^{2+} release rates than the near-neutral MEM solution.

$$ZnO + 2H^+ \leftrightarrow Zn^{2+} + H_2O \quad (6)$$

$$ZnO + H_2O \leftrightarrow Zn^{2+} + 2OH^- \quad (7)$$

3.3. *In vitro cytotoxicity*

THP-1 human monocytes were exposed to PLA and its nanocomposites for 1, 3, and 7 days. Additionally, a commercially available antibacterial PLA-Ag filament with the tradename Bioguard was used as a comparative material for the cytotoxic profiles of the nanocomposites produced in this study. Cytotoxicity was measured using a cell viability assay known as the MTS assay. Unexposed cells were employed as the negative control, while cells exposed to 5% DMSO were used as the positive cytotoxicity control of this study. In accordance with ISO 10993-5 [80], a reduction in the relative cell viability below 70% of the untreated control indicates a potential cytotoxic effect of the tested materials. The positive control (5% DMSO) distinctly exhibited its cytotoxic effect at all three exposure times that was consistent with previous experiments, with percentage cell viabilities of 5% DMSO relative to the unexposed group of: 43.3% ± 0.4% (day 1), 24.7% ± 1.9% (day 3), and 20.6% ± 0.9% (day 7), confirming the validity of the experimental set up. Pristine PLA was non-cytotoxic, with percentage cell viabilities relative to the unexposed group of: 90.7% ± 3.1% (day 1), 86.2% ± 2.2% (day 3), and 99.5% ± 2.8% (day 7), such that the cytotoxic levels of PLA were also statistically similar to the unexposed group throughout the experimental duration. The average percentage cell viability of PLA on each day was then assigned a nominal cell viability of 100 %, which was subsequently used to determine the relative cell viabilities of Bioguard and the nanocomposites, as shown in Fig. 6.

Among the experimental groups, only the nanocomposites with the

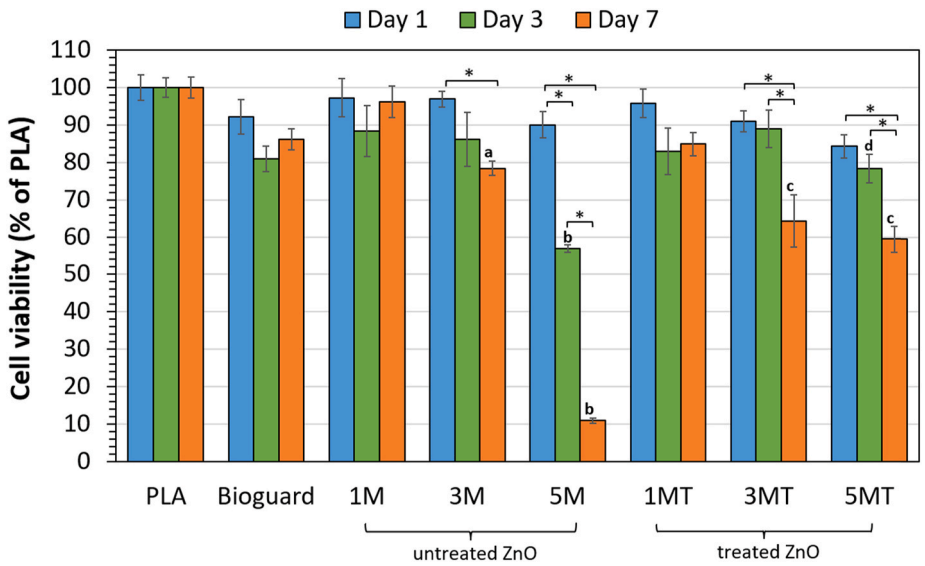

Fig. 6. Cell viability of human THP-1 monocytes after 1, 3, and 7 days of exposure to test materials (data expressed as the mean ± SEM of four replicates). Notes: * significantly different between exposure periods within a treatment group; [a] 3M was significantly different to PLA on day 7; [b] significantly different to all the groups of the same exposure period; [c] significantly different to all the groups of the same exposure period except among 5MT, 3MT and 3M; [d] 5MT was significantly different to PLA on day 3.

highest filler loadings, namely 5M (untreated ZnO) on day 3 and 7, and 5MT (treated ZnO) on day 7, clearly indicated cytotoxic effects as they possessed cell viability mean values with SEMs wholly below 70% of the untreated control cell viability (Fig. 6). By the end of the experiment, the cytotoxicity of 5M was statistically similar to the 5% DMSO positive control group. Other experimental groups showed minimal potential cytotoxicity as their means and SEMs maintained above 70% cell viability throughout the exposure period.

Monocytes are key players in the immune system, and so THP-1 monocytes are commonly used to assess ZnO cytotoxicity since they are among the first cells to encounter nanoparticles in the body [81–85]. As previously mentioned, most of the ZnO nanoparticles were embedded in the polymer matrix, suggesting that the release of Zn^{2+}, rather than the release of ZnO nanoparticles, primarily drives cytotoxicity. Indeed, it is well known that excessive concentrations of Zn^{2+} can be toxic, despite its vital role of in cellular functions under normal conditions [86–88]. While the exact cytotoxic mechanism of ZnO is not fully understood, it is known that cytotoxicity primarily arises from nanoparticle internalisation and the subsequent intracellular dissolution of Zn^{2+} [81–83]. Notably, extracellular Zn^{2+} alone is insufficient to induce significant cytotoxic effects [81,83,89], partly due to its tendency to form poorly soluble zinc-carbonate-phosphate precipitates in serum-containing cell culture media [81].

Nevertheless, the extracellular Zn^{2+} concentration, estimated from the Zn^{2+} release data in MEM (Table S1), is crucial since it directly influences cellular uptake. MEM closely matches the composition and pH of the cell culture medium used for the cytotoxicity tests, although lower nanoparticle solubility is expected in the serum-containing media [83]. It is important to note that the extracellular Zn^{2+} measured after acid digestion via ICP-MS includes contribution from both intact nanoparticles and ionic species, making it difficult to discern their respective proportions [90]. Nonetheless, Shen et al. [81] showed that the form of Zn, be it the ZnO particles or the Zn^{2+} ionic species, did not significantly impact the degree of cytotoxicity on THP-1 cells.

According to Section 3.2, the differences in Zn^{2+} release from the nanocomposites during the 7-day cell viability test (~2–47 mg/mL (168 h) (Table S1)) were not statistically significant, yet they influenced the cytotoxicity profiles. For instance, 5M showed significantly lower cell viabilities than the other nanocomposites after both 3 days (72 h) and 7 days (168 h) of exposure (Fig. 6), releasing approximately double and quintuple the concentration of Zn^{2+} compared to the others (Table S1). This suggests that a threshold concentration of released Zn^{2+} is required for the nanocomposites to elicit dose- and time-dependent cytotoxic responses, consistent with previous studies showing that excessing the threshold for *in vitro* concentrations can overwhelm cellular pathways and lead to apoptosis [81–83].

Importantly, silanisation only significantly impacted cytotoxicity at the highest filler loading. Specifically, ZnO treatment in 5MT significantly lowered both the Zn^{2+} release rates and the extent of cytotoxic effects, leading to statistically similar cell viability levels to the rest of the materials after 3 days of cell exposure. Interestingly, while not evident in this study, silane coating may induce cytotoxicity by increasing the surface charge of the nanoparticles due to positively charged amine groups [91,92]. Positively charged surfaces tend to favour the adsorption of serum proteins and biomolecules, creating a layer known as the 'protein corona' around the nanoparticles, which facilitates cellular uptake and potentially increases cytotoxicity [93–95]. However, the effect of the protein corona on cytotoxicity remains debated; some studies suggest it may actually reduce cytotoxicity [96,97]. These conflicting results likely arise from the varying involvement of different protein types in the internalisation process, as certain proteins do not contribute to cellular uptake [94].

From Fig. 6, it is clear that both treated and untreated ZnO nanofillers increased the cytotoxicity of PLA in a concentration- and time-dependent manner after exceeding the Zn^{2+} threshold concentration. Throughout the experiment, the samples with the lowest filler loadings, 1M (untreated ZnO) and 1MT (treated ZnO), showed comparable cytotoxicity to pristine PLA.

In comparison with Bioguard, pristine PLA appeared less cytotoxic, though statistical significance was not reached at any of the incubation times. According to the supplier's datasheet [5], the Ag additive in Bioguard comprises less than 2% of the total material composition, but it is unclear whether this is by weight or volume as no further specifications were provided. The lack of detailed information on the type of Ag additive, the filler loading, and the fabrication methodology for Bioguard complicates direct comparisons with cytotoxic effects of the ZnO nanofillers.

Nevertheless, the results indicate that the cytotoxicity of Bioguard on THP-1 cells over 7 days is comparable to the nanocomposites with filler loadings < 5 wt% for untreated ZnO and < 3 wt% for treated ZnO.

Notably, the cell viabilities of Bioguard were statistically similar to those of 1M, 1MT, and 3M throughout the experiment, while 5M after 3 days and both 3MT and 5MT after 7 days were statistically more cytotoxic.

3.4. Antibacterial properties

The antibacterial properties of PLA and its nanocomposites were evaluated against the gram-positive bacteria strain *S. aureus*, and the gram-negative bacteria strain *E. coli*. Additionally, the antibacterial performance of the commercially available Bioguard was used as a benchmark. The antibacterial indices calculated on a log scale with respect to PLA are presented in Fig. 7. Notably, materials with antibacterial indices > 2 are considered "antibacterial", indicating > 99% reduction in the bacterial population [25,31].

According to the literature, several mechanisms can contribute to the antibacterial properties of ZnO, and these include the release of reactive oxygen species (ROS), the release of Zn^{2+}, the disruption of cell membranes, and the internalisation of nanoparticles [88,98,99]. However, the predominant mode of action is still debated as it is largely dependent on physical properties such as the morphology and size of ZnO particles [100].

Despite being embedded in PLA, ZnO nanofillers retained good antibacterial properties at around 3 wt% filler loading in conventionally manufactured structures [12,25,31]. However, this study demonstrated that excellent antibacterial properties (> 99% of bacteria reduction) were achieved even at filler loadings below 3 wt%, as shown in Fig. 7. The enhanced antibacterial efficacy of the printed parts likely arises from their higher porosity compared to conventional manufactured components such as compression-moulded samples. The μCT analysis of our previous study showed that the printed nanocomposite samples had porosity between 11% and 19%, similar to the 18% of printed PLA [21], while compression-moulded samples exhibited negligible porosity.

During the degradation tests, the open porosity of the printed samples increased the specific surface area for interaction with the immersion medium, resulting in faster degradation rates than the nearly pore-free conventional specimens [101]. This increased degradation rate facilitates the release of Zn^{2+} and ZnO, both critical for antibacterial activity, which explains why the printed samples in this study achieved excellent antibacterial responses at filler loadings lower than those typically reported in the literature.

The antibacterial effects of ZnO-containing nanocomposites primarily stem from the combined action of ZnO nanoparticles and Zn^{2+} ions [25,102]. This hypothesis aligns with our preliminary qualitative test results from the disk diffusion method, which showed no inhibition zones due to the poor solubility of ZnO in the agar, limiting the diffusion of Zn^{2+} to induce any antibacterial effects, as already discussed by Sevinç and Hanley [103]. Moreover, the antibacterial contribution of Zn^{2+} was also confirmed when limited antibacterial effects were detected when we used nutrient broth as the test medium, as the antibacterial action of Zn^{2+} was hindered by the interactions with protein-based organic compounds, as observed by Rewak-Soroczynska et al. [104]. Therefore, H_2O was chosen as the test medium, as it minimised the interference of protein compounds while ensuring that the bacteria remained sufficiently viable to evaluate the antibacterial properties of the nanocomposites.

Overall, the results indicate that the antibacterial efficacy of the nanocomposites was stronger against *E. coli* than *S. aureus* (Fig. 7). Notably, 5M appeared to be more effective against *S. aureus*, but this was due to *E. coli* reaching a maximum antibacterial index of 5.2 after complete elimination at 24 h. *E. coli* was more sensitive to nutrient deprivation in H_2O, resulting in slight growth reduction in the control population, which contributed to a lower index compared to *S. aureus* (6.9). Fig. 7 actually shows that 5M eliminated both bacteria after 24 h.

The varying susceptibility of these bacteria to the antibacterial properties of PLA-ZnO nanocomposites is well-documented, with conflicting findings in the literature. Some studies report higher antibacterial efficacy against gram-positive bacteria [12,24,105], while others suggest greater effectiveness against gram-negative bacteria [25,106]. This discrepancy arises from the difference in sensitivity of the two bacteria to the different antibacterial mechanisms of ZnO. For instance, membrane disruption may be more effective against *E. coli* due to its thinner cell wall [107], while negatively charged ROS ions generated by ZnO photoactivation may penetrate *S. aureus* more effectively due to its less negatively charged membrane [108]. Additionally, the chemical structure of PLA, particularly its ester groups, can influence antibacterial activity by contributing to electrostatic repulsion with negatively charged bacteria [14]. The overall susceptibility of the bacteria is thus dependent on the dominating antibacterial mode of action.

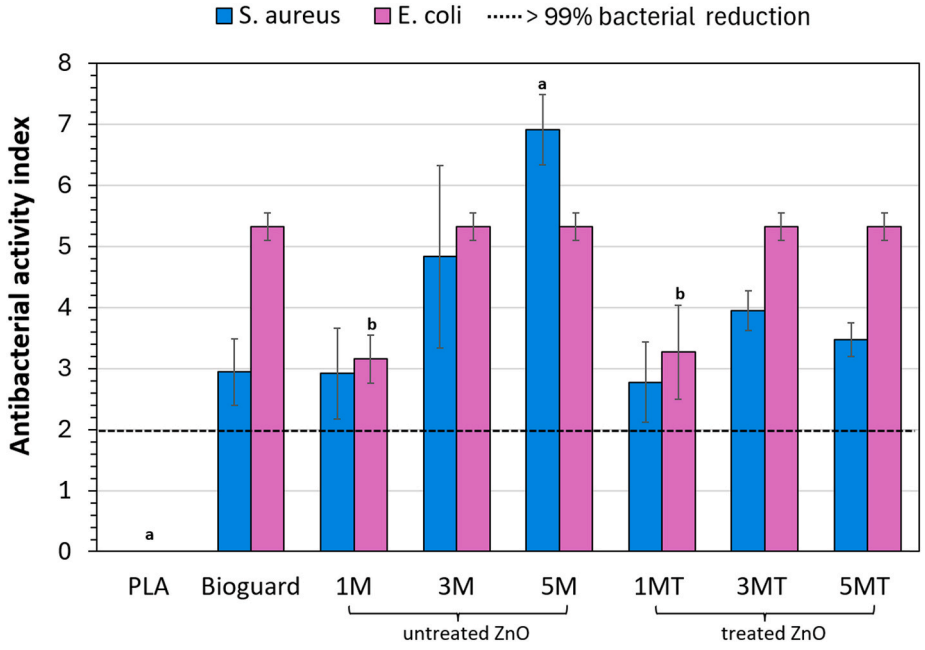

Fig. 7. Antibacterial activity of the different materials in this study towards *S. aureus* and *E. coli* after 1 day of incubation (data expressed as the mean ± SEM of three replicates). [a] significantly different to all other groups for *S. aureus*, [b] significantly different to all other groups for *E.coli*, except between 1M and 1 MT.

As mentioned above, the antibacterial effects of the nanocomposites primarily rely on the ZnO and Zn^{2+} released into the medium. The concentrations of these components in the test medium can be approximated from the Zn^{2+} release data in H_2O in Section 3.2 (Table S2). The detailed effect of the filler loading and the surface treatment on the degradation rates, and thus the Zn^{2+} release rates governing the antibacterial properties, have been elaborated in Section 3.1.

While the differences in the Zn^{2+} concentration released after 24 h were not statistically significant compared to the total concentration released over 12 weeks, they were sufficient to differentiate antibacterial capabilities. Antibacterial indices (Fig. 7) increased with higher released Zn^{2+} concentrations (Table S2), but only nanocomposites achieving maximum indices: 5.2 for *E. coli* and 6.9 for *S. aureus*, were statistically more effective. All nanocomposites showed > 99% bacterial reduction, but only a few, such as 5M for *S. aureus* and 3M, 3MT, 5M, and 5MT for *E. coli*, completely eliminated the bacteria. Minimum Zn^{2+} concentrations for complete eradication varied by strain: approximately 13.7 mg/mL for *S. aureus* and 4.2 mg/mL for *E. coli* (Table S2).

The commercial product Bioguard completely eliminated the *E. coli* population, demonstrating comparable efficacy to PLA-ZnO nanocomposites with filler loadings > 3 wt%. However, Bioguard was less effective against *S. aureus*, exhibiting efficacy comparable to the lowest filler loadings (1M and 1MT) (Fig. 7). Only 5M was statistically more antibacterial against *S. aureus* than Bioguard. The stronger antibacterial action of Bioguard against the gram-negative strain aligns with the literature indicating that gram-negative bacteria are generally more susceptible to Ag^+ ions, likely due the tendency of Ag^+ adherence to their negatively charged lipopolysaccharide layer [109–112]. Overall, it can be concluded that the antibacterial efficacy of Bioguard was comparable to the nanocomposites with filler loadings of > 3 wt% for *E. coli* and < 5 wt% for *S. aureus*.

3.5. Determination of optimum material composition

This study determines the optimal material composition of PLA-ZnO nanocomposites for FFF printing of antibacterial biomedical devices by analysing their ability to balance between printability, antibacterial properties, and biocompatibility. Preliminary assessments of printability and mechanical properties were published in a separate study [21]. Building on those findings, this study examines the effects of filler loading and filler treatment on the antibacterial efficacy and biocompatibility of the nanocomposites.

While all nanocomposites exhibited desirable antibacterial effects, only those remaining non-cytotoxic are suitable for biomedical applications. Cytotoxicity results on day 1 (after 24 h of incubation) indicated that all nanocomposites were non-cytotoxic and had cell viabilities statistically similar to that of PLA. However, longer exposure periods revealed dose- and time-dependent cytotoxicity, with nanocomposites containing higher filler loadings becoming potentially cytotoxic from day 1 to day 7. By the end of the cytotoxicity tests, only the 1M and 1MT formulations, with the lowest filler loadings, demonstrated comparable cytotoxicity levels to PLA throughout the duration of the study. These findings suggest that incorporating 1 wt% to 2 wt% of ZnO nanofiller can achieve effective antibacterial properties without compromising biocompatibility.

By combining insights from our previous study on printability [21] with the current research on biological properties, we determined that using melt-mixed masterbatches, effective filler treatment (silanisation), and incorporating 1 wt% to 2 wt% of ZnO nanoparticles strikes an ideal balance between printability, mechanical properties, and antibacterial performance. This formulation achieved over a 99% reduction in bacterial populations while maintaining cell viability comparable to pristine PLA. Ultimately, 1MT emerged as the optimal candidate for 3D printing applications in biomedical devices.

3.6. Limitations

This study presents several limitations to consider when interpreting the findings. A key limitation is that the antibacterial and biocompatibility tests were conducted under different conditions, specifically, the antibacterial assessments utilised H_2O as the test inoculum, while the biocompatibility evaluations employed RPMI 1640. Both antibacterial activity and cyto-compatibility in human cells serve as measures of relative *in vitro* cytotoxicity, with accurate determination requiring optimal experimental conditions and cell proliferation assays tailored to each target biological system (i.e., gram-positive and gram-negative bacterial strains or human cells). Despite these differences, consistent Zn^{2+}release profiles offer a valuable correlation between the two results. Zn^{2+} release tests were conducted in acidified H_2O and MEM, closely simulating the respective testing environments. Notably, both media exhibited no significant differences in released Zn^{2+} concentrations across the two experimental periods. The results indicate that Zn^{2+} is a primary contributor to both antibacterial and cytotoxic responses. Its release is strongly related to the concentration of the filler, which is the main variable affecting the release of Zn^{2+}. While this correlation links the antibacterial and biocompatibility results, further investigation is needed to fully understand their interplay. Future studies should standardise test conditions for both antibacterial and biocompatibility assessments to enhance comparability.

Moreover, while this study establishes a foundational framework for assessing the biological properties of the nanocomposites, more in-depth evaluations, such as long-term studies, assessments with a broader range of cell lines and bacteria, and *in vivo* experiments, are recommended. Standardising conditions like pH and exposure duration, along with increasing sample sizes, will ensure repeatable and reliable results, ultimately confirming the safety and effectiveness of the nanocomposites for biomedical applications.

4. Conclusion

This study determined the viability of 3D printed PLA-ZnO nanocomposites to be adopted in healthcare settings through a detailed assessment of their biological properties. To this aim, the biodegradability, antibacterial activity, and cytotoxicity of 3D printed PLA-ZnO nanocomposites containing 1 wt% to 5 wt% of either treated or untreated fillers were systematically investigated.

Findings revealed that the antibacterial and cytotoxic properties of the nanocomposites were governed by the combined effects of ZnO and Zn^{2+} released from the matrix, which varied with filler loading and surface treatment.

1. Effect of Filler Loading: Higher filler loading increased matrix degradation, leading to higher Zn^{2+} release rates. While this enhanced antibacterial efficacy (> 99% reduction in bacteria), it also increased the extent of cytotoxicity in THP-1 cells. Nanocomposites with < 5 wt% loading provided excellent antibacterial properties while remaining non-cytotoxic.
2. Effect of Silane Treatment: Silane treatment reduced ZnO nanoparticle hydrophilicity, which in turn decreased PLA degradation and Zn^{2+} release rates. This effect was influenced by filler loading, as increased PLA crystallinity countered the decrease in hydrophilicity. Overall, silane treatment did not significantly alter antibacterial properties or cytotoxicity, except at high filler loadings, where it lowered cytotoxicity due to decreased Zn^{2+} release.

By fine-tuning filler loading and surface treatment, this study demonstrated that ZnO nanoparticles can enhance the antibacterial properties of PLA without negatively impacting its biocompatibility. Ultimately, nanocomposites with < 2 wt% silane-treated ZnO nanoparticles were identified as the most viable choice for additive manufacturing of antibacterial PLA-ZnO nanocomposites for biomedical

applications.

CRediT authorship contribution statement

Wei Juene Chong: Writing – review & editing, Writing – original draft, Validation, Methodology, Investigation, Formal analysis, Data curation. **Paul Wright:** Writing – review & editing, Methodology, Investigation, Formal analysis, Data curation. **Dejana Pejak Simunec:** Methodology, Investigation. **Srinivasan Jayashree:** Investigation. **Winston Liew:** Investigation. **Chad Heazlewood:** Writing – review & editing, Investigation. **Adrian Trinchi:** Conceptualization. **Ilias (Louis) Kyratzis:** Conceptualization. **Yuncang Li:** Conceptualization. **Shirley Shen:** Conceptualization. **Antonella Sola:** Writing – review & editing, Resources, Methodology, Funding acquisition, Conceptualization. **Cuie Wen:** Writing – review & editing, Resources, Methodology, Funding acquisition, Conceptualization.

Data availability

Data will be made available upon request.

Declaration of competing interest

The authors declare that they have no known competing financial interests or personal relationships that could have appeared to influence the work reported in this paper. The author Antonella Sola is an Associate Editor and the author Cuie Wen is the Editor in Chief for ***Smart Materials in Manufacturing*** and were not involved in the editorial review or the decision to publish this article.

Acknowledgements

CW, YL and PW are supported by the Australian Research Council (ARC) through the discovery grant DP210101862.

The authors would like to acknowledge Terry Turney from Micronisers Pty. Ltd. for supplying the ZnO nanoparticles used in this project.

The authors would like to acknowledge the Department of Medicine, University of Melbourne for supplying the human acute monocytic leukemia (THP-1) cell line used for the *in vitro* cytotoxicity test.

The authors would like to acknowledge Nicola Spencer and Megan Kruger at the Chromatography Facility in CSIRO Manufacturing for their contribution to the analytical chromatography analysis in Section 3.1.

Appendix A. Supplementary data

Supplementary data to this article can be found online at https://doi.org/10.1016/j.smmf.2024.100069.

References

[1] Additive Manufacturing General principles - Fundamentals and Vocabulary, ISO/ASTM 52900, Nov. 2021. [Online]. Available: https://www.iso.org/standard/74514.html.
[2] S.H. Masood, Advances in Fused deposition modeling, in: S. Hashmi, G. F. Batalha, C.J. Van Tyne, B. Yilbas (Eds.), Comprehensive Materials Processing, Elsevier, 2014, pp. 69–91.
[3] Copper 3D, Plactive. https://copper3d.com/producto/plactive/, (accessed July 17, 2024).
[4] 3D Universe, Cicla 3D nano-infused copper antibacterial PLA filament 1.75mm (1kg). https://shop3duniverse.com/products/cicla-3d-antibacterial-pla-filament-1-75mm-1kg#v32771069149238. (Accessed 17 July 2024).
[5] 3DXTECH, Bioguard antibacterial PLA 3D filament. https://www.3dxtech.com/wp-content/uploads/2021/10/BioGuard_PLA_SDS_v1.0.pdf. (Accessed 17 July 2024).
[6] Smart Materials 3D, Innovatefil antibacterial. https://www.smartmaterials3d.com/en/antibacterial. (Accessed 17 July 2024).
[7] A. Almatroudi, Silver nanoparticles: synthesis, characterisation and biomedical applications, Open Life Sci. 15 (2020) 819–839.
[8] K. Gudikandula, S. Charya Maringanti, Synthesis of silver nanoparticles by chemical and biological methods and their antimicrobial properties, J. Exp. Nanosci. 11 (2016) 714–721.
[9] J. Hou, H. Liu, L. Wang, L. Duan, S. Li, X. Wang, Molecular toxicity of metal oxide nanoparticles in Danio rerio, Environ. Sci. Technol. 52 (2018) 7996–8004.
[10] S. Naz, A. Gul, M. Zia, Toxicity of copper oxide nanoparticles: a review study, IET Nanobiotechnol. 14 (2020) 1–13.
[11] R. Ridwan, T. Rihayat, S. Suryani, A.S. Ismi, N. Nurhanifa, S. Riskina, Combination of poly lactid acid zinc oxide nanocomposite for antimicrobial packaging application, IOP Conf. Ser. Mater. Sci. Eng. 830 (2020) 042018.
[12] D. Kim, V. Karthika, K. Gopinath, K. Sadeghi, S. Thanakkasaranee, J. Seo, Poly (lactic acid)/ZnO bionanocomposite films with positively charged ZnO as potential antimicrobial food packaging materials, Polym 11 (2019) 1427.
[13] S.M. Rashedi, R. Khajavi, A. Rashidi, M.K. Rahimi, A. Bahador, Novel PLA/ZnO nanofibrous nanocomposite loaded with tranexamic acid as an effective wound dressing: in vitro and in vivo assessment, Iran, J. Biotechnol. 19 (2021) 38–47.
[14] W.J. Chong, S. Shen, Y. Li, A. Trinchi, D. Pejak, I.L. Kyratzis, A. Sola, C. Wen, Additive manufacturing of antibacterial PLA-ZnO nanocomposites: benefits, limitations and open challenges, J. Mater. Sci. Technol. 111 (2022) 120–151.
[15] R. Kumar, R. Singh, M. Singh, P. Kumar, ZnO nanoparticle-grafted PLA thermoplastic composites for 3D printing applications: tuning of thermal, mechanical, morphological and shape memory effect, J. Thermoplast. Compos. Mater. 35 (2022) 799–825.
[16] J. Junpha, A. Wisitsoraat, R. Prathumwan, W. Chaengsawang, K. Khomungkhun, K. Subannajui, Electronic tongue and cyclic voltammetric sensors based on carbon nanotube/polylactic composites fabricated by fused deposition modelling 3D printing, Mater. Sci. Eng. C 117 (2020) 111319.
[17] R. Singh, R. Kumar, M. Singh, P. Kumar, P. Preet, On mechanical, thermal, morphological and shape memory effect of sol-gel prepared ZnO nanoparticle reinforced PLA composites materials, Proc. Natl. Acad. Sci. India Sect. A (Phys. Sci.) 92 (2022) 699–712.
[18] Z. Brounstein, C.M. Yeager, A. Labouriau, Development of antimicrobial PLA composites for fused filament fabrication, Polymers 13 (2021) 580.
[19] T. Jamnongkan, O. Jaroensuk, A. Khankhuean, A. Laobuthee, N. Srisawat, A. Pangon, R. Mongkholrattanasit, P. Phuengphai, A. Wattanakornsiri, C.-F. Huang, A comprehensive evaluation of mechanical, thermal, and antibacterial properties of PLA/ZnO nanoflower biocomposite filaments for 3D printing application, Polym 14 (2022) 600.
[20] A. Anžlovar, A. Kržan, E. Žagar, Degradation of PLA/ZnO and PHBV/ZnO composites prepared by melt processing, Arab. J. Chem. 11 (2018) 343–352.
[21] W.J. Chong, D.P. Simunec, A. Trinchi, I.L. Kyratzis, Y. Li, P. Wright, S. Shen, A. Sola, C. Wen, Advancing the additive manufacturing of PLA-ZnO nanocomposites by fused filament fabrication, Virtual Phys. Prototyp. 19 (2024) e2285418.
[22] M. Murariu, S. Benali, Y. Paint, A.-L. Dechief, O. Murariu, J.-M. Raquez, P. Dubois, Adding value in production of multifunctional polylactide (PLA)-ZnO nanocomposite films through alternative manufacturing methods, Molecules 26 (2021) 2043.
[23] Y.A. Arfat, J. Ahmed, A. Al Hazza, H. Jacob, A. Joseph, Comparative effects of untreated and 3-methacryloxypropyltrimethoxysilane treated ZnO nanoparticle reinforcement on properties of polylactide-based nanocomposite films, Int. J. Biol. Macromol. 101 (2017) 1041–1050.
[24] A.S. Doumbia, H. Vezin, M. Ferreira, C. Campagne, E. Devaux, Studies of polylactide/zinc oxide nanocomposites: influence of surface treatment on zinc oxide antibacterial activities in textile nanocomposites, J. Appl. Polym. Sci. 132 (2015) 41776.
[25] R. Pantani, G. Gorrasi, G. Vigliotta, M. Murariu, P. Dubois, PLA-ZnO nanocomposite films: water vapor barrier properties and specific end-use characteristics, Eur. Polym. J. 49 (2013) 3471–3482.
[26] NatureWorks, Ingeo biopolymer 3D850 technical data sheet. https://www.natureworksllc.com/~/media/Files/NatureWorks/Technical-Documents/Technical-Data-Sheets/TechnicalDataSheet_3D850_monofilament_pdf.pdf?la=en. (Accessed 17 July 2024).
[27] Micronisers, Nanosun zinc oxide P99/30. https://www.micronisers.com/nanosun-zinc-oxide-p99-30/. (Accessed 17 July 2024).
[28] S. Dash, P. Murthy, L. Nath, P. Chowdhury, Kinetic modeling on drug release from controlled drug delivery systems, Acta Pol. Pharm. 67 (2010) 217–223.
[29] S.J. O'Keefe, B.N. Feltis, T.J. Piva, T.W. Turney, P.F.A. Wright, ZnO nanoparticles and organic chemical UV-filters are equally well tolerated by human immune cells, Nanotoxicology 10 (2016) 1287–1296.
[30] Biomérieux Industry, Quality control microorganisms. https://www.biomerieux-usa.com/sites/subsidiary_us/files/quality-control-microorganisms-catalog-1.pdf. (Accessed 17 July 2024).
[31] M. Murariu, A. Doumbia, L. Bonnaud, A.L. Dechief, Y. Paint, M. Ferreira, C. Campagne, E. Devaux, P. Dubois, High-performance Polylactide/ZnO nanocomposites designed for films and fibers with special end-use properties, Biomacromolecules 12 (2011) 1762–1771.
[32] F. Iñiguez-Franco, R. Auras, J. Ahmed, S. Selke, M. Rubino, K. Dolan, H. Soto-Valdez, Control of hydrolytic degradation of poly(lactic acid) by incorporation of chain extender: from bulk to surface erosion, Polym. Test. 67 (2018) 190–196.
[33] G.L. Robertson, Food packaging, in: N.K. Van Alfen (Ed.), Encyclopedia of Agriculture and Food Systems, Academic Press, Oxford, 2014, pp. 232–249.
[34] J.C. Middleton, A.J. Tipton, Synthetic biodegradable polymers as orthopedic devices, Biomaterials 21 (2000) 2335–2346.

[35] B. van Bochove, D.W. Grijpma, Photo-crosslinked synthetic biodegradable polymer networks for biomedical applications, J. Biomater. Sci. Polym. Ed. 30 (2019) 77–106.
[36] C. Bode, H. Kranz, A. Fivez, F. Siepmann, J. Siepmann, Often neglected: PLGA/PLA swelling orchestrates drug release: HME implants, J. Contr. Release 306 (2019) 97–107.
[37] S. Lyu, D. Untereker, Degradability of polymers for implantable biomedical devices, Int. J. Mol. Sci. 10 (2009) 4033–4065.
[38] S. Hurrell, R.E. Cameron, The effect of buffer concentration, pH and buffer ions on the degradation and drug release from polyglycolide, Polym. Int. 52 (2003) 358–366.
[39] S. Li, H. Garreau, M. Vert, Structure-property relationships in the case of the degradation of massive poly(α-hydroxy acids) in aqueous media, J. Mater. Sci. Mater. Med. 1 (1990) 198–206.
[40] J. Vazquez-Armendariz, R. Tejeda-Alejandre, A. Rodriguez-Garcia, Y.I. Vega-Cantu, C. Mendoza-Buenrostro, C.A. Rodriguez, Influence of controlled cooling on crystallinity of poly(l-lactic acid) scaffolds after hydrolytic degradation, Materials 13 (2020) 2943.
[41] M.I. Tayouri, S. Estaji, S.R. Mousavi, S. Salkhi Khasraghi, R. Jahanmardi, S. Nouranian, M. Arjmand, H.A. Khonakdar, Degradation of polymer nanocomposites filled with graphene oxide and reduced graphene oxide nanoparticles: a review of current status, Polym. Degrad. Stabil. 206 (2022) 110179.
[42] E. Trofimchuk, V. Ostrikova, O. Ivanova, M. Moskvina, A. Plutalova, T. Grokhovskaya, A. Shchelushkina, A. Efimov, E. Chernikova, S. Zhang, V. Mironov, Degradation of structurally modified polylactide under the controlled composting of food waste, Polym 15 (2023) 4017.
[43] D. Huang, Z.-D. Hu, T.-Y. Liu, B. Lu, Z.-C. Zhen, G.-X. Wang, J.-H. Ji, Seawater degradation of PLA accelerated by water-soluble PVA, E-Polymers 20 (2020) 759–772.
[44] M. Treiser, S. Abramson, R. Langer, J. Kohn, Degradable and resorbable biomaterials, in: B.D. Ratner, A.S. Hoffman, F.J. Schoen, J.E. Lemons (Eds.), Biomaterials Science, third ed., Academic Press, 2013, pp. 179–195.
[45] L.N. Woodard, M.A. Grunlan, Hydrolytic degradation and erosion of polyester biomaterials, ACS Macro Lett. 7 (2018) 976–982.
[46] A. Sola, W.J. Chong, D.P. Simunec, Y. Li, A. Trinchi, I.L. Kyratzis, C. Wen, Open challenges in tensile testing of additively manufactured polymers: a literature survey and a case study in fused filament fabrication, Polym. Test. 117 (2023) 107859.
[47] M. Qu, H. Tu, M. Amarante, Y.Q. Song, S.S. Zhu, Zinc oxide nanoparticles catalyze rapid hydrolysis of poly(lactic acid) at low temperatures, J. Appl. Polym. Sci. 131 (2014) 40287.
[48] R. Puglisi, A.A. Scamporrino, N.T. Dintcheva, G. Filippone, E. Bruno, P. Scarfato, P. Cerruti, S.C. Carroccio, Photo- and water-degradation phenomena of ZnO bio-blend based on Poly(lactic acid) and Polyamide 11, Polym 15 (2023) 1434.
[49] N. Follain, S. Belbekhouche, J. Bras, G. Siqueira, S. Marais, A. Dufresne, Water transport properties of bio-nanocomposites reinforced by Luffa cylindrica cellulose nanocrystals, J. Membr. Sci. 427 (2013) 218–229.
[50] S. Sugiman, S. Salman, M. Maryudi, Effects of volume fraction on water uptake and tensile properties of epoxy filled with inorganic fillers having different reactivity to water, Mater, Today Commun. 24 (2020) 101360.
[51] D.A. Goncharova, E.N. Bolbasov, A.L. Nemoykina, A.A. Aljulaih, T. S. Tverdokhlebova, S.A. Kulinich, V.A. Svetlichnyi, Structure and properties of biodegradable PLLA/ZnO composite membrane produced via electrospinning, Materials 14 (2021) 2.
[52] R. Zhang, W. Lan, T. Ji, D.E. Sameen, S. Ahmed, W. Qin, Y. Liu, Development of Polylactic acid/ZnO composite membranes prepared by ultrasonication and electrospinning for food packaging, Lebensm. Wiss. Technol. 135 (2021) 110072.
[53] S. Mallakpour, M. Hatami, Bionanocomposites preparation and characterization: dispersion of surface-modified ZnO nanoparticles in optically active poly(Amide-Imide) derived from 3,5-diamino-N-(4-hydroxyphenyl)benzamide and amino acid, Des. Monomers Polym. 14 (2011) 461–473.
[54] C. Zou, J.C. Fothergill, S.W. Rowe, The effect of water absorption on the dielectric properties of epoxy nanocomposites, IEEE Trans. Dielectr. Electr. Insul. 15 (2008) 106–117.
[55] L. Masaro, X.X. Zhu, Physical models of diffusion for polymer solutions, gels and solids, Prog. Polym. Sci. 24 (1999) 731–775.
[56] H. Tsuji, C.A. Del Carpio, In vitro hydrolysis of blends from enantiomeric poly (lactide)s. 3. homocrystallized and amorphous blend films, Biomacromolecules 4 (2003) 7–11.
[57] C. Wolf, H. Angellier-Coussy, N. Gontard, F. Doghieri, V. Guillard, How the shape of fillers affects the barrier properties of polymer/non-porous particles nanocomposites: a review, J. Membr. Sci. 556 (2018) 393–418.
[58] M. van Essen, R. Thür, M. Houben, I.F.J. Vankelecom, Z. Borneman, K. Nijmeijer, Tortuous mixed matrix membranes: a subtle balance between microporosity and compatibility, J. Membr. Sci. 635 (2021) 119517.
[59] M. Vert, S.M. Li, H. Garreau, Attempts to map the structure and degradation characteristics of aliphatic polyesters derived from lactic and glycolic acids, J. Biomater. Sci. Polym. Ed. 6 (1995) 639–649.
[60] J. Schley Lyu, B. Loy, D. Lind, C. Hobot, R. Sparer, D. Untereker, Kinetics and time-temperature equivalence of polymer degradation, Biomacromolecules 8 (2007) 2301–2310.
[61] A.M. Reed, D.K. Gilding, Biodegradable polymers for use in surgery -poly (glycolic)/poly(lactic acid) homo and copolymers: 2. In vitro degradation, Polym 22 (1981) 494–498.
[62] M. Gerometta, J.R. Rocca-Smith, S. Domenek, T. Karbowiak, Physical and chemical stability of PLA in food packaging, in: Reference Module in Food Science, Elsevier, 2019.
[63] R. Vaid, E. Yildirim, M.A. Pasquinelli, M.W. King, Hydrolytic degradation of Polylactic acid fibers as a function of pH and exposure time, Molecules 26 (2021) 7554.
[64] M.C. Araque-Monrós, A. Vidaurre, L. Gil-Santos, S. Gironés Bernabé, M. Monleón-Pradas, J. Más-Estellés, Study of the degradation of a new PLA braided biomaterial in buffer phosphate saline, basic and acid media, intended for the regeneration of tendons and ligaments, Polym. Degrad. Stabil. 98 (2013) 1563–1570.
[65] D. Penkov, P. Lukova, H. Manev, S. Dimitrova, M. Kassarova, Polymer tablet matrix systems for the controlled release of dry Betula Pendula leaf extract, Polym 15 (2023) 3558.
[66] D.L.A. Sitta, M.R. Guilherme, E.P. da Silva, A.J.M. Valente, E.C. Muniz, A. F. Rubira, Drug release mechanisms of chemically cross-linked albumin microparticles: effect of the matrix erosion, Colloids Surf. B Biointerfaces 122 (2014) 404–413.
[67] F. Ganji, S. Vasheghani Farahani, E. Vasheghani-Farahani, Theoretical description of hydrogel swelling: a review, Iran. Polym. J. (Engl. Ed.) 19 (2010) 375–398.
[68] S. Maity, B. Sa, Ca-carboxymethyl xanthan gum mini-matrices: swelling, erosion and their impact on drug release mechanism, Int. J. Biol. Macromol. 68 (2014) 78–85.
[69] B. Almería, T.M. Fahmy, A. Gomez, A multiplexed electrospray process for single-step synthesis of stabilized polymer particles for drug delivery, J. Contr. Release 154 (2011) 203–210.
[70] J. Siepmann, A. Göpferich, Mathematical modeling of bioerodible, polymeric drug delivery systems, Adv. Drug Deliv. Rev. 48 (2001) 229–247.
[71] A.N. Ford Versypt, D.W. Pack, R.D. Braatz, Mathematical modeling of drug delivery from autocatalytically degradable PLGA microspheres - a review, J. Contr. Release 165 (2013) 29–37.
[72] X. Zhu, R.D. Braatz, A mechanistic model for drug release in PLGA biodegradable stent coatings coupled with polymer degradation and erosion, J. Biomed. Mater. Res. A. 103 (2015) 2269–2279.
[73] K. Sevim, J. Pan, A mechanistic model for acidic drug release using microspheres made of PLGA 50:50, Mol. Pharm. 13 (2016) 2729–2735.
[74] A. Adrover, C. Venditti, M. Giona, Swelling and drug release in polymers through the theory of Poisson–Kac stochastic processes, Gels 7 (2021) 32.
[75] J. Varshosaz, M. Hajian, Characterization of drug release and diffusion mechanism through Hydroxyethylmethacrylate/Methacrylic acid pH-sensitive hydrogel, Drug Deliv. 11 (2004) 53–58.
[76] N. Wu, L.-S. Wang, D.C.-W. Tan, S.M. Moochhala, Y.-Y. Yang, Mathematical modeling and in vitro study of controlled drug release via a highly swellable and dissoluble polymer matrix: polyethylene oxide with high molecular weights, J. Contr. Release 102 (2005) 569–581.
[77] A. Göpferich, Mechanisms of polymer degradation and erosion, in: D.F. Williams (Ed.), The Biomaterials: Silver Jubilee Compendium, Elsevier Science, Oxford, 1996, pp. 117–128.
[78] D. Cardoso, A. Narcy, S. Durosoy, Y. Chevalier, The pH dependence of dissolution kinetics of zinc oxide, Colloids Surf., A 650 (2022) 129653.
[79] P. Schindler, H. Althaus, W. Feitknecht, Löslichkeitsprodukte von Metalloxiden und -hydroxiden. 9. Mitteilung. Löslichkeitsprodukte und Freie Bildungsenthalpien von Zinkoxid, amorphem Zinkhydroxid, β11-, β2-, γ-, δ- und ϵ-Zinkhydroxid, Helv. Chim. Acta 47 (1964) 982–991.
[80] Biological Evaluation of Medical Devices - Part 5: Tests for in Vitro Cytotoxicity, ISO 10993, Jun. 2009 [Online]. Available: https://www.iso.org/standard/36406.html.
[81] C. Shen, S.A. James, M.D. de Jonge, T.W. Turney, P.F.A. Wright, B.N. Feltis, Relating cytotoxicity, Zinc ions, and reactive oxygen in ZnO nanoparticle-exposed human immune cells, Toxicol. Sci. 136 (2013) 120–130.
[82] B.N. Feltis, S.J. O'Keefe, A.J. Harford, T.J. Piva, T.W. Turney, P.F.A. Wright, Independent cytotoxic and inflammatory responses to zinc oxide nanoparticles in human monocytes and macrophages, Nanotoxicology 6 (2012) 757–765.
[83] M. Luo, C. Shen, B.N. Feltis, L.L. Martin, A.E. Hughes, P.F.A. Wright, T.W. Turney, Reducing ZnO nanoparticle cytotoxicity by surface modification, Nanoscale 6 (2014) 5791–5798.
[84] V.A. Senapati, A. Kumar, G.S. Gupta, A.K. Pandey, A. Dhawan, ZnO nanoparticles induced inflammatory response and genotoxicity in human blood cells: a mechanistic approach, Food Chem. Toxicol. 85 (2015) 61–70.
[85] D. Sahu, G.M. Kannan, M. Tailang, R. Vijayaraghavan, In vitro cytotoxicity of nanoparticles: a comparison between particle size and cell type, J. Nanosci. 2016 (2016) 4023852.
[86] Y. Liu, L. Wang, X. Dou, M. Du, S. Min, B. Zhu, X. Liu, Osteogenesis or apoptosis-twofold effects of Zn^{2+} on bone marrow mesenchymal stem cells: an in vitro and in vivo study, ACS Omega 9 (2024) 10945–10957.
[87] J. Ma, N. Zhao, D. Zhu, Bioabsorbable zinc ion induced biphasic cellular responses in vascular smooth muscle cells, Sci. Rep. 6 (2016) 26661.
[88] W.J. Chong, S. Shen, Y. Li, A. Trinchi, D.P. Simunec, I.L. Kyratzis, A. Sola, C. Wen, Biodegradable PLA-ZnO nanocomposite biomaterials with antibacterial properties, tissue engineering viability, and enhanced biocompatibility, Smart Materials in Manufacturing. 1 (2023) 100004.
[89] T.W. Turney, M.B. Duriska, V. Jayaratne, A. Elbaz, S.J. O'Keefe, A.S. Hastings, T. J. Piva, P.F.A. Wright, B.N. Feltis, Formation of Zinc-containing nanoparticles from Zn2+ ions in cell culture media: implications for the nanotoxicology of ZnO, Chem. Res. Toxicol. 25 (2012) 2057–2066.

[90] Z. Khabir, A.M. Holmes, Y.-J. Lai, L. Liang, A. Deva, M.A. Polikarpov, M. S. Roberts, A.V. Zvyagin, Human epidermal Zinc concentrations after topical application of ZnO nanoparticles in sunscreens, Int. J. Mol. Sci. 22 (2021) 12372.
[91] F. Grasset, N. Saito, D. Li, D. Park, I. Sakaguchi, N. Ohashi, H. Haneda, T. Roisnel, S. Mornet, E. Duguet, Surface modification of zinc oxide nanoparticles by aminopropyltriethoxysilane, J. Alloys Compd. 360 (2003) 298–311.
[92] M. Amano, H. Shibata, K. Hashimoto, Crystal growth of HAp on plate-like ZnO particles using APTES as surface treatment agents, J. Asian Ceram. Soc. 11 (2023) 53–61.
[93] R. Bilardo, F. Traldi, A. Vdovchenko, M. Resmini, Influence of surface chemistry and morphology of nanoparticles on protein corona formation, WIREs Nanomed. Nanobio. 14 (2022) e1788.
[94] Y. Arezki, F. Delalande, C. Schaeffer-Reiss, S. Cianférani, M. Rapp, L. Lebeau, F. Pons, C. Ronzani, Surface charge influences protein corona, cell uptake and biological effects of carbon dots, Nanoscale 14 (2022) 14695–14710.
[95] E. Froehlich, The role of surface charge in cellular uptake and cytotoxicity of medical nanoparticles, Int. J. Nanomed. 7 (2012) 5577–5591.
[96] V. Forest, M. Cottier, J. Pourchez, Electrostatic interactions favor the binding of positive nanoparticles on cells: a reductive theory, Nano Today 10 (2015) 677–680.
[97] Y. Lee, E.-J. Choi, T. Webster, S.-H. Kim, D. Khang, Effect of the protein corona on nanoparticles for modulating cytotoxicity and immunotoxicity, Int. J. Nanomed. (10) (2014) 97–113.
[98] B.L. da Silva, M.P. Abuçafy, E.B. Manaia, J.A. Oshiro Junior, B. Chiari-Andréo, R. C.L.R. Pietro, L.A. Chiavacci, Relationship between structure and antimicrobial activity of Zinc oxide nanoparticles: an overview, Int. J. Nanomed. 14 (2019) 9395–9410.
[99] K.S. Siddiqi, A. ur Rahman, Tajuddin, A. Husen, Properties of zinc oxide nanoparticles and their activity against microbes, Nanoscale Res. Lett. 13 (2018) 141.
[100] N. Babayevska, Ł. Przysiecka, I. Iatsunskyi, G. Nowaczyk, M. Jarek, E. Janiszewska, S. Jurga, ZnO size and shape effect on antibacterial activity and cytotoxicity profile, Sci. Rep. 12 (2022) 8148.
[101] V. Chandran, J. Kalman, K. Fayazbakhsh, H. Bougherara, A comparative study of the tensile properties of compression molded and 3D printed PLA specimens in dry and water saturated conditions, J. Mech. Sci. Technol. (2021) 1977–1985.
[102] A. Al-Jumaili, P. Mulvey, A. Kumar, K. Prasad, K. Bazaka, J. Warner, M.V. Jacob, Eco-friendly nanocomposites derived from geranium oil and zinc oxide in one step approach, Sci. Rep. 9 (2019) 5973.
[103] B.A. Sevinç, L. Hanley, Antibacterial activity of dental composites containing zinc oxide nanoparticles, J. Biomed. Mater. Res. B Appl. Biomater. 94B (2010) 22–31.
[104] J. Rewak-Soroczynska, A. Dorotkiewicz-Jach, Z. Drulis-Kawa, R.J. Wiglusz, Culture media composition influences the antibacterial effect of silver, cupric, and zinc ions against Pseudomonas Aeruginosa, Biomolecules 12 (2022) 963.
[105] H. Rodríguez-Tobías, G. Morales, A. Ledezma, J. Romero, D. Grande, Novel antibacterial electrospun mats based on poly(d,l-lactide) nanofibers and zinc oxide nanoparticles, J. Mater. Sci. 49 (2014) 8373–8385.
[106] H. Zhang, M. Hortal, M. Jordá-Beneyto, E. Rosa, M. Lara-Lledo, I. Lorente, ZnO-PLA nanocomposite coated paper for antimicrobial packaging application, Lebensm. Wiss. Technol. 78 (2017) 250–257.
[107] V.V. Shinde, D.S. Dalavi, S.S. Mali, C.K. Hong, J.H. Kim, P.S. Patil, Surfactant free microwave assisted synthesis of ZnO microspheres: study of their antibacterial activity, Appl. Surf. Sci. 307 (2014) 495–502.
[108] T. Gordon, B. Perlstein, O. Houbara, I. Felner, E. Banin, S. Margel, Synthesis and characterization of zinc/iron oxide composite nanoparticles and their antibacterial properties, Colloids Surf., A 374 (2011) 1–8.
[109] M. Godoy-Gallardo, U. Eckhard, L.M. Delgado, Y.J.D. de Roo Puente, M. Hoyos-Nogués, F.J. Gil, R.A. Perez, Antibacterial approaches in tissue engineering using metal ions and nanoparticles: from mechanisms to applications, Bioact. Mater. 6 (2021) 4470–4490.
[110] T.C. Dakal, A. Kumar, R. Majumdar, V. Yadav, Mechanistic basis of antimicrobial actions of silver nanoparticles, Front. Microbiol. 7 (2016) 1831.
[111] A.V. Domínguez, R.A. Algaba, A.M. Canturri, Á.R. Villodres, Y. Smani, Antibacterial activity of colloidal silver against gram-negative and gram-positive bacteria, Antibiotics 9 (2020) 36.
[112] T.D. Tavares, J.C. Antunes, J. Padrão, A.I. Ribeiro, A. Zille, M.T.P. Amorim, F. Ferreira, H.P. Felgueiras, Activity of specialized biomolecules against gram-positive and gram-negative bacteria, Antibiotics 9 (2020) 314.